Inorganica Chimica Acta 390 (2012) 210–216

Contents lists available at SciVerse ScienceDirect

Inorganica Chimica Acta

journal homepage: www.elsevier.com/locate/ica

Synthesis, characterization and distinct butyrylcholinesterase activities of transition metal complexes of 2-[(*E*)-(quinolin-3-ylimino)methyl]phenol

Muhammad Ikram [a,b], Saeed-Ur-Rehman [a,*], Sadia Rehman [a], Robert J. Baker [b], Carola Schulzke [b]

[a] Institute of Chemical Sciences, University of Peshawar, Pakistan
[b] School of Chemistry, University of Dublin, Trinity College Dublin 2, Ireland

ARTICLE INFO

Article history:
Received 10 February 2012
Received in revised form 15 April 2012
Accepted 23 April 2012
Available online 3 May 2012

Keywords:
Transition metal complexes
X-ray single crystal diffraction
Acetylcholinesterase and
butyrylcholinesterase inhibition activities

ABSTRACT

2-[(*E*)-(Quinolin-3-ylimino)methyl]phenol (H-QMP) was synthesized by condensing salicylaldehyde with 2-aminoquinoline and fully characterized by mass spectrometry, ^{1}H and $^{13}C\{^{1}H\}$NMR, and IR spectroscopies. The metal complexes $[M(QMP)(OAc)]H_2O$ where M = Cu(II) and Zn(II) and $[M(QMP)_2]$ where M = Ni and Co(II) were prepared from the metal acetates. All transition metal complexes were assigned geometries based on the UV–Vis spectra, conductivity and magnetic susceptibilities. $[M(QMP)_2]$, {where M = Ni and Co(II)}, were further characterized by single crystal X-ray diffraction and were found to be pseudo-octahedral with interquinoline interaction to the metal center. The complexes were screened for acetylcholinesterase (AChE) and butyrylcholinesterase (BChE). Only cobalt and copper containing complexes were found to be active against BChE with IC_{50} = 69 ± 0.0112 and 5 ± 0.0004 μM ± SEM, respectively. Surprisingly no activity was observed for AChE, therefore selective BChE inhibition was observed for copper and cobalt complexes only.

1. Introduction

Alzheimer's disease (AD) is a degenerative brain disease, which destroys the neurons and the connections to the cerebral cortex and causes dementia which progresses from short term memory loss to complete immobility [1]. Dementous neurofibrillary tangles are probably caused by the oxidative effects of lipids [2–4]. Amyloid beta (Aβ or Abeta) is a peptide linkage of 36–43 amino acids and appears to be the main constituent of amyloid plaques found in the brains of patients with Alzheimer's disease. Aβ is involved in oxidative stress of the lipids found in the cell membranes of the tissues which ultimately lead to dementia. The hydrolysis reaction as shown in Scheme 1 below takes place at the catalytic site, of which the residue serine 200 (Ser-200) is an integral part.

Inhibition of acetylcholinesterase is considered as a promising approach for the treatment of Alzheimer's disease (AD) and for possible therapeutic applications in the treatment of Parkinson's disease, ageing, and myasthenia gravis [5,6]. Meanwhile, butyrylcholinesterase (BChE) has been considered to be directly associated with the side effects of the acetylcholinesterase (AChE) inhibitors and the existing drugs for Alzheimer Disease (AD) [7]. More recent studies have shown that BChE is found in significantly higher quantities in AD plaques than in the plaques of age related non-demented brains. Other relevant studies have also reported that the unfavorable side effect profile of AChE inhibitors are not associated with their poor selectivity towards AChE [8]. To overcome AD, drugs have been developed which prevent the hydrolysis of the acetylcholine by blocking the acetylcholinesterase (AChE). Acetylcholinesterase inhibitors (AChEIs) prevent the acylation of the hydroxyl group of Ser200. Reported AChEIs are (−)-Huprine, Tacrine, and Hup A Dimers (Fig. 1) [9–21].

Furthermore, it was found that the brain requires high metal ion [Cu(II), Zn(II) and Fe(III)] concentrations for numerous essential functions. In Alzheimer's patients the metal ion homeostasis is severely deregulated. The metals are not aggregates but only part of these i.e. they accumulate in the form of Aβ aggregates in dementia and hence stressful oxidative processes are triggered. Therapies, which are currently used for overcoming the oxidative stress, include (i) ameliorating or inhibiting Aβ aggregation and induced Reactive Oxygen Species (ROS) generation, (ii) use of antioxidants and (iii) use of metal chelators. Clioquinol metal complexes are found to be the most promising drugs in AD treatment. Despite the human trials for clioquinol drugs already taking place, the mode of action is still not clear [22]. Our interest in investigating AChE and BChE inhibition came from the study carried out by Budimir et al. of the metal based drugs of this important class of ligands. According to them, ligands of such class can take part in metal exchange reactions which will ultimately lead to decrease in Aβ plaques [22]. It was also found that metal chelators of the N, O-type with an aromatic environment can easily cross the blood brain barrier and can cause the formation of metalated rings including aromatic properties with Aβ plaques. The ab initio DFT of various aromatic ligands toward copper complexation studies

* Corresponding author. Tel.: +92 321 90 20756.
E-mail address: srachem@yahoo.com (Saeed-Ur-Rehman).

0020-1693/$ - see front matter © 2012 Elsevier B.V. All rights reserved.
http://dx.doi.org/10.1016/j.ica.2012.04.036

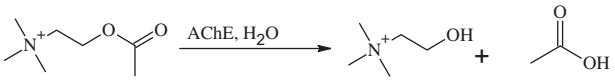

Scheme 1. Hydrolysis of ACh by AChE.

carried out by Sodupe et al. show that increasing the sigma donating property of the ligand might affect the therapeutic activity of the complexes [22]. In the H-QMP ligand the quinoline nitrogen is increasing the electron density of the ring and hence the covalency toward transition metal ions. It was also found to offer opportunities for inducing substrate chirality and reorientations in geometry around the metal center, thereby tuning the metal's electronic structure. Metal complexes of Ni(II), Co(II), Cu(II) and Zn(II) were synthesized by condensing with H-QMP as ligand precursor. The metals are not aggregates but only part of these i.e. they accumulate in the form of Aβ aggregates in dementia, therefore these metal complexes are supposed to be active in overcoming the oxidative stress of metal ion accumulation in Aβ aggregation. The brain of Alzheimer patients show that metal ions present inside the body accumulate in plaques which consequently produce hydrogen peroxide causing damage to the brain. Previously it was reported that metal complexes containing copper aggregate the senile plaque more efficiently than any other metal complex [23]. Here, we extended the research in this field to certain other metal ions such as cobalt(II) and nickel(II).

These metal complexes will potentially lead to increased metal ion concentration through exchange processes and decreased senile plaques. This study should be of great importance in the exploration of metal based drugs for neurological disorders.

2. Experimental

2.1. Materials and methods

All chemicals, buffers and solvents used were of analytical grade. Metal(II) acetates (where metal(II) = Co, Ni, Cu and Zn) were obtained from Riedel-de-Haen, and were partially dehydrated by drying the hydrated salts in a vacuum oven for several hours at 80–100 °C. 3-aminoquinoline was obtained from Sigma Aldrich whereas salicylaldehyde was obtained from Acros Organics. Solvents were distilled at least twice before use. Electric eel acetylcholinesterase, horse serum butyrylcholinesterase, acetylthiocholine iodide, butyrylthiocholine chloride, 5,5′-thiobis-2-nitrobenzoic acid (DTNB) and eserine were purchased from Sigma. Unless otherwise stated, all reactions were carried out under a dinitrogen atmosphere.

2.2. Instrumentation

Elemental analyses were carried out on Varian Elementar II. The metal ion content in all samples was carried out by atomic absorption spectrophotometer (Vario 6, Analytic Jena). The instrument was operated on single beam mode. The concentration of each metal was determined against standard calibration curve with regression value (R2) of 0.9997 obtained with commercial standards (CPA Chem. Ltd., Bulgaria). Melting points were recorded on a Gallenkamp apparatus. IR spectra were recorded using Shimadzo FTIR Spectrophotometer Prestige-21. ^{1}H NMR were measured with Bruker DPX 400 MHz (400.23 MHz) whereas, ^{13}C{^{1}H} NMR were recorded on Bruker AV 400 MHz (150.9 MHz) spectrometers in $CDCl_3$ at room temperature. Chemical shifts are reported in ppm and standardized by observing signals for residual protons. UV–Vis spectra were recorded on a BMS UV-1602. Molar conductance of the solutions of the metal complexes was determined with a conductivity meter type HI-8333. All measurements were carried out at room temperature with freshly prepared solutions. Magnetic susceptibilities were measured on a Sherwood Gouy Balance at room temperature calibrated with $Hg[Co(SCN)_4]$. Mass spectra were recorded on a LCT Orthogonal Acceleration TOF Electrospray mass spectrometer. Single crystal analyses were carried out using Rigaku Saturn-724 diffractometer (graphite-monochromated Mo Kα radiation, λ = 0.71073 Å) at 108(2) K.

2.3. Synthesis of 2-[(E)-(quinolin-3-ylimino)methyl]phenol (H-QMP)

Salicylaldehyde (1.2 cm^3, 0.011 mol) was added to a solution of 3-aminoquinoline (1.6 g, 0.011 mol) in ethanol which was stirred for 3 h. An orange solution was obtained and concentrated using rotary evaporator. The product was purified by washing with 10% copious *n*-hexane and methanol solution. (Yield: 1.5 g, 55%). M.p. 190–191 °C. IR: 3200(bd), 1591(s), 1554(s), 1492(s), 1381w, 1361(s), 1338(s), 1319(w), 1280(s), 1224(s), 1203(s), 1165(s), 1109(s), 927(s), 900(s), 848(s), 798(s), 780(s), 750(s), 736(s), 638(s), 610(w) cm^{-1}. ^{1}H NMR (400.23 MHz, CD_3OD, 303 k):

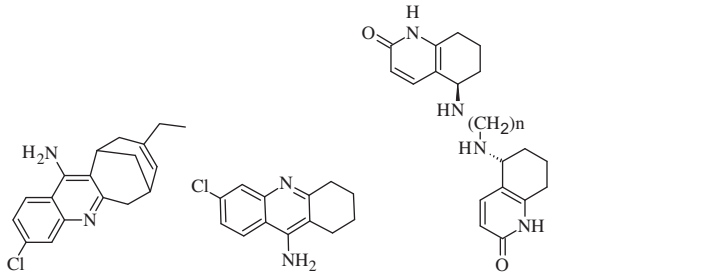

(-)-Huprine Tacrine Hup A Dimers where n = 10 & 12

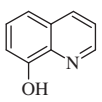

Cliquinol

Fig. 1. Drugs used for treating Alzheimer Disease.

δ = 11.0 (s, 1H, Ar-OH), 9.0 (s, 1H, –HC=N), 8.8 (s, 1H, H2), 8.10 (d, $^3J_{HH}$ = 8.35 Hz, 1H, H9), 8.0 (s,1H, H4), 7.8 (d, $^3J_{HH}$ = 7.72 Hz, 1H, H6), 7.73 (d, $^3J_{HH}$ = 7.9 Hz, 1H, H8), 7.70 (t, $^3J_{HH}$ = 7.55 Hz, 1H, H16), 7.4 (m, 1H, H17), 7.3 (d, $^3J_{HH}$ = 7.6, 1H, H18), 7.1 (d, $^3J_{HH}$ = 8.03 Hz, 1H, H15), 7.0 (d, $^3J_{HH}$ = 7.48 Hz, 1H, H7) ppm, $^{13}C\{^1H\}$ NMR (150.9 MHz, CD_3OD, 303k), 165(HC=N–, C12), 162 (aromatic C–OH, C14), 147 (C, C10), 146 (CH, C2), 142 (C, C5), 134 (CH, C15), 133 (CH, C18), 129.4 (CH, C17), 129.2 (CH, C16), 128 (C, C3), 127.8 (CH, C6), 127.4 (CH, C7), 124.7 (CH, C8), 116 (CH, C9) ppm. *Anal.* Calc. for $C_{16}H_{12}N_2O$: C, 77.40; H, 4.87; N, 11.28. Exp.: C, 76.80; H, 5.10; N, 10.89%. EI-MS: *m*/*z* (%) 249.1017 (100%) $[C_{16}H_{12}N_2O^+]$.

2.4. Synthesis of $[M(QMP)_2]$ where M = Ni and Co(II) acetates

0.011 mol of metal(II) acetates were stirred in a minimum volume of dried methanol and 0.024 mol of H-QMP in a minimum volume of dried methanol was added to the metal solution. The mixture was stirred for 2–3 h at room temperature. The metal complex was collected after filtration and copiously washed several times with 5% *n*-hexane containing methanol.

2.5. Bis(2-[(E)-(quinolin-3-ylimino)methyl]phenolato)nickel(II) (**1**)

X-ray quality crystals were formed by slow diffusion of dichloromethane and diethyl ether. After three days dark green diamond shaped single crystals appeared. IR: 1612(s), 1558(s), 1537(s), 1496(s), 1471(s), 1444(s), 1388(w), 1369(s), 1321(s), 1220(w), 1155(s), 1136(w), 1124(s), 1035(s), 999(w), 898(s), 819(s), 810(s), 750(s), 732(s), 636(s), 596(w) cm^{-1}. λ_{max} = 720 nm (ε = 27.7 M^{-1} cm^{-1}, $^1A_{1g} \rightarrow {}^1A_{2g}$). μ_{eff}: 2.7 B.M. *Anal.* Calc. for $C_{32}H_{22}N_4O_2Ni$: C, 69.47; H, 4.01; N, 10.13; Ni, 10.61. Exp.: C, 70.43; H, 3.88; N, 11.56; Ni, 10.50%. EI-MS: *m*/*z* (%) 554.2787 (15%) $[C_{32}H_{22}N_4O_2Ni^+ + 2H^+]$, 249.5734 (100%) $[C_{16}H_{12}N_2O^+]$, 145.3759 (5%) $[C_9H_8N_2^+]$, $\otimes_m$ = 0.01 S cm^{-1}.

2.6. Bis(2-[(E)-(quinolin-3-ylimino)methyl]phenolato)cobalt(II) (**2**)

IR analysis: 2800–3300(bd), 1656(w), 1604(s), 1533(s), 1500(s), 1419(w), 1338(s), 1236(s), 1192(s), 1120(s), 1029(s), 980(s), 894(s), 800(w), 752(s), 667(s), 650(s) cm^{-1}. λ_{max} = 640 nm (ε = 16.6 M^{-1} cm^{-1}, $^2A_{2g} \rightarrow {}^2B_{1g}$), μ_{eff}: 4.4 B.M. *Anal.* Calc. for $C_{32}H_{22}N_4O_2Co$: C, 69.44; H, 4.01; N, 10.12; Co, 10.65. Exp.: C, 68.66; H, 4.23; N, 9.68; Co, 11.12%. MS-ES$^+$: *m*/*z* (%) 553.1060 (48%) $[C_{32}H_{22}N_4O_2Co^+]$, 249.1078 (100%) $[C_{16}H_{12}N_2O^+]$, 145.1128 (10%) $[C_9H_8N_2^+]$, $\otimes_m$ = 0.03 S cm^{-1}.

2.7. Synthesis of $[M(QMP)(CH_3COO)]H_2O$ where M = Cu and Zn(II) acetates

0.011 mol of metal(II) acetates was stirred in a minimum volume of dried methanol to which 0.011 mol of H-QMP in a minimum volume of dried methanol was added. The mixture was stirred for 2–3 h at room temperature. In metal salts containing water of crystallization excess dimethoxy propane was added for dehydrating and the solution was stirred for 3 h at room temperature under nitrogen before adding the ligand. The metal complex was collected after filtration and washed many times with n-hexane containing methanol.

2.8. 2-[(E)-(Quinolin-3-ylimino)methyl]phenolatoacetatoaquocopper (II) (**3**)

IR analysis: 3290(bd), 1729(w), 1604(s), 1555(s), 1480(s), 1360(s), 1338(s),1280(w), 1200(s), 1160(w), 980(s), 848(s), 750(s), 650(s) cm^{-1}. λ_{max} = 850 nm (ε = 19.3 M^{-1} cm^{-1}, $^2E \rightarrow {}^2T_2$). μ_{eff}: 4.5 B.M. *Anal.* Calc. for $C_{18}H_{16}N_2O_4Cu$: C, 55.74; H, 4.16; N, 7.22; Cu, 16.38. Exp.: C, 55.44; H, 4.10; N, 8.22; Cu, 15.88%. MS-ES: *m*/*z* (%) = 387.8771 (10%) $[C_{18}H_{16}N_2O_4Cu^+]$, (90%) $[C_{16}H_{12}N_2O^+]$, $\otimes_m$ = 0.01 S cm^{-1}.

2.9. 2-[(E)-(Quinolin-3-ylimino)methyl]phenolatoacetatoaquozinc(II) (**4**)

IR analysis: 3000–3400(bd), 1734(w), 1606(s), 1568(s), 1492(w), 1361(s), 1338(s), 1280(s), 1203(s), 1165(s), 977(s), 848(s), 750(s), 638(s) cm^{-1}. *Anal.* Calc. for $C_{18}H_{16}N_2O_4Zn$: C, 55.47; H, 4.14; N, 7.19; Zn, 16.78. Exp.: C, 55.74; H, 4.10; N, 7.22; Zn, 16.38%. MS-ES: *m*/*z* (%) = 389.7396 (5%) $[C_{18}H_{16}N_2O_4Zn^+]$, 249.110 (100%) $[C_{16}H_{12}N_2O^+]$, 145.1200 (2%) $[C_9H_8N_2^+]$, $\otimes_m$ = 0.01 S cm^{-1}.

2.10. AChE and BChE inhibition assay

AChE Inhibition was determined spectrophotometrically, with acetylthiocholine as substrate, by modifying the method reported by Ellman [24]. The reaction was carried out in 100 μM sodium phosphate buffer (pH 8.0) at 25 °C. In a typical assay, 140 μl of buffer, 20 μl of enzyme preparation (final concentration 0.037 U/ml in 0.1 M phosphate buffer solution), and 20 μl (0.05 mM) of metal compound solution were mixed and incubated for 30 min. Ten microliters (0.15 mM) of 5,5′-dithio-bis-nitrobenzoic acid (DTNB) was added, and the reaction was initiated by adding 10 μl of acetylthiocholine. Butyrylthiocholine chloride was used as a substrate to assay BChE under similar conditions as above. The rates of hydrolysis of acetylthiocholine and butyrylthiocholine were determined by monitoring the formation of the yellow 2-nitro-5-sulfanylbenzoate anion (as a result of the reaction of DTNB with the thiocholine released by the enzymatic hydrolysis) at a wavelength of 412 nm. Methanol was used as negative control. Galanthamine dissolved in methanol was used as standard drug at 10 μg/ml concentrations. All the reactions were performed in triplicate in 96-well microplates in Spectrmax 340 (Molecular Devices, USA).

2.11. Determination of IC_{50} values

The concentrations of test compounds that inhibited the hydrolysis of substrates (acetylthiocholine and butyrylthiocholine) by 50% (IC_{50}) were determined by monitoring the effect of increasing concentrations of these compounds on the inhibition values. The IC_{50} values were then calculated using the EZ-Fit Enzyme Kinetics program (Perrella Scientific Inc., Amherst, USA).

2.12. Crystal structure determination

Suitable single crystals for X-ray structural analyses of **1** and **2** were mounted on a glass fiber, and the respective data were collected on a Rigaku Saturn-724 diffractometer (graphite-monochromated Mo Kα radiation, λ = 0.71073 Å) at 108(2) K. The structures were solved by direct methods (SHELXS-97) and refined against all data by full-matrix least-squares methods on F^2 (SHELXL-97) [25]. All non-hydrogen-atoms were refined with anisotropic displacement parameters. The hydrogen atoms were refined isotropically on calculated positions using a riding model with their U_{iso} values constrained to 1.5 U_{eq} of their pivot atoms for terminal sp^3 carbon atoms and 1.2 times for all other carbon atoms.

3. Results and discussion

The ligand H-QMP was synthesized by condensing salicylaldehyde with 3-aminquinoline to yield the phenolic Schiff base ligand.

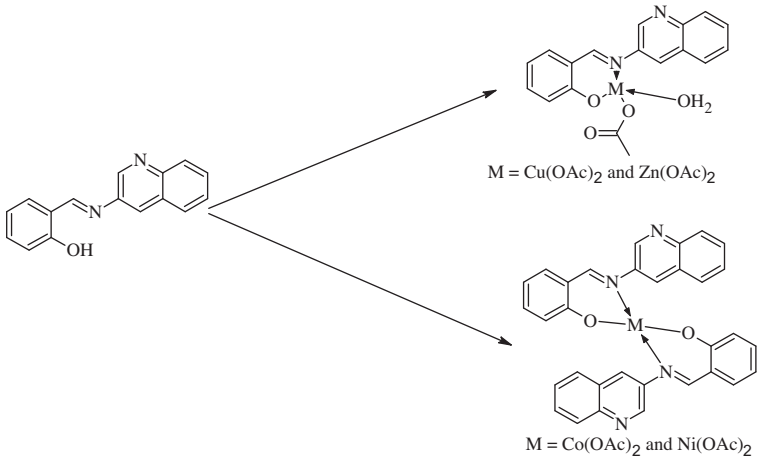

Scheme 2. Metal complexation by H-QMP.

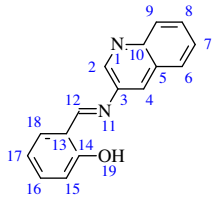

Scheme 3. Atoms numbering used for NMR signals.

This was characterized by ^{1}H and $^{13}C\{^{1}H\}$ NMR spectroscopy which shows the expected resonances. The ^{1}H and $^{13}C\{^{1}H\}$ NMR peaks were assigned on the basis of Scheme 3. Two singlets observed upfield at δ_H = 11.0 ppm δ_H = 9.0 ppm are assigned to the –HC=N– and phenolic protons, respectively. The remaining NMR spectrum shows the region for aromatic protons. The $^{13}C\{^{1}H\}$ spectrum also shows the azomethine peak at 165 ppm and the Ar–C–OH peak at 162 ppm, respectively. The aromatic resonances were explicitly assigned in the ^{1}H and $^{13}C\{^{1}H\}$ spectra. The ligand H-QMP was reacted with the divalent metal ions of Ni, Co, Cu and Zn as shown in Scheme 2. The elemental composition of the ligand and metal complexes were unambiguously determined and reported which suggest the proposed composition for all compounds. This is further supported by ESI(+) mass spectrometry. Due to paramagnetic nature of the metal complexes of H-QMP ligand, the NMR recorded for all the complexes show broad unidentifiable peaks, therefore results were not presented. All the complexes were found to be non-electrolyte in nature confirming coordination of the OAc^{-} ligands in **3** and **4**.

Since the IR spectra of all metal complexes are quite similar, the discussion is confined to the most important vibrations in the region of 4000–600 cm^{-1} in relation to the structure. The free ligand IR spectrum shows a broad peak around 3400 cm^{-1}, which is assigned to the –OH stretch. This absorption region either decreases in size or broadens to a large extent upon complexation with metal ions. Coordinated water in case of **3** and **4** shows a similar absorption band. The sharp band in the H-QMP spectrum at 1624 cm^{-1} is assigned to the $\nu_{(C=N)}$ vibration mode which was found to be shifting by the difference of $\Delta\nu_{(C=N)}$ = 10–30 cm^{-1} in metal complexes. In **3** and **4** the C=O stretch for the coordinated acetate ion is observed at 1729 and 1734 cm^{-1}, respectively. The C-O stretch of acetate is observed at 1280 cm^{-1} for both complexes **3** and **4**.

Except for the zinc complex all complexes show magnetic moments for spin only values. For **1**, **2**, and **3** the magnetic moment values suggest that the complexes are high spin.

The UV–Vis spectra of compounds **1**, **2**, and **3** were measured in the region of 200–1000 nm. These spectra show only one absorption band each for all of the compounds viz.; for **1** the major absorption at 720 nm was assigned to a transition $^{1}A_1g \rightarrow {}^{1}A_2g$ since the other charge transfer bands caused by $^{1}A_1g \rightarrow {}^{1}B_1g$ and $^{1}A_1g \rightarrow Eg$ transitions are expected to be observed in the lower absorption region. However, no significant absorption of this kind was observed in rigorously purified samples, possibly because these transitions are buried beneath the absorption region for $^{1}A_1g \rightarrow {}^{1}A_2g$. The 2.7 B.M. $\mu_{effective}$ value and the absorption band in the visible region confirm that the crystal field splitting between sets of d*yz*, d*zx* and dz^2 orbitals and d*xy* and $dx^2 - y^2$ orbitals is large. Furthermore, the energies of the d*xy* and $dx^2 - y^2$ orbitals ($\Delta E = 1.73 \times 10^{-3}$ eV) are similar enough to allow for their occupation with one single electron each. The splitting of orbitals is shown in Fig. 2.

It was concluded by Gray and Ballhausen that for ligand-to-metal transitions (exhibited unambiguously by complexes without an intraligand π system) the two charge-transfer bands are separated by nearly 10000 cm^{-1}, whereas for metal-to-ligand transitions (shown by complexes with an intraligand π system), the three charge-transfer bands shown by nickel square planar complexes are more closely spaced (approximately 2000–3000 cm^{-1} apart) [25,26]. The metal complexes formed with the aromatic monoanionic ligand H-QMP are therefore expected to yield transitions which will overlap in a narrow range.

For **2** the absorption occurs at 640 nm which was tentatively assigned to the $^{2}A_{2g} \rightarrow {}^{2}B_{1g}$ transition on the basis of the 16.6 M^{-1} cm^{-1} molar extinction coefficient value. It was presumed that for the C_{2v} symmetry of the cobalt complex the $^{2}A_{2g} \rightarrow {}^{2}B_{1g}$ transition is allowed whereas $^{2}A_2 \rightarrow {}^{2}A_1$ is forbidden. The 4.4 B.M. $\mu_{effective}$ value and the visible absorption band for **2** show that the dyz and dzx set of orbitals and the dz^2, d*xy*, $dx^2 - y^2$ set of orbitals are spaced closely. The crystal filed splitting ($\Delta E = 1.93 \times 10^{-3}$ eV) between dz^2 and the d*xy*, $dx^2 - y^2$ set of orbitals is not very high as compared to complex **1** (see Fig. 2). Therefore each of dz^2 and d*xy* orbitals are occupied by a single electron resulting in a high spin cobalt complex. For **3** the visible band observed at 850 nm is assigned to the $^{2}E \rightarrow {}^{2}T_2$ tetrahedral transition.

All transitions are assigned to the excitation from pπ electrons from the phenolate ion to dπ* orbitals of the metal ion. The imine-nitrogen also donates pπ electrons to the dπ* orbital of the metal ion leading to transitions, which were presumed to be occurring in the region of 500–700 nm. However, these bands are obscured by the more intense phenolate to metal ion transitions [25].

3.1. Structural analyses

Both **1** and **2** crystallize from dichloromethane/ether solutions at room temperature in the monoclinic space group $P2_1/c$, with one half of the symmetric monomer in the asymmetric unit (Figs. 3 and 4). The structures of both complexes are, except for the central metal, identical. Therefore we are refraining from an in-depth study of the individual structures except where the difference is apparent enough to warrant discussion and instead focus predominantly on the structural evaluation of **1**. The ORTEP plots for **1** and **2** show that both central metals are coordinated by two ligands in *trans* fashion generating an almost perfect square planar coordination geometry (nickel and cobalt lie directly in the N_2O_2 plane with no deviation from it). The O(1)–M–O(1A) and N(1)–M–N(1A) [where M = Ni(II), and Co(II)] bond angles are (due to the space group symmetry) exactly 180° and emphasize coplanarity (Fig. 3). The O(1)–Ni(1)–N(1) is only slightly deviated from a perfect right angle with 90.37°. The small difference of the bond angles C(1)–O(1)–Ni(1) (125.19°) and N(1)–C(7)–Ni(1) (120.87°) shows that the chelate ring formed by the anionic ligands and the metal is not symmetrical. This is further evidenced by the dihedral angle of 28.48° between the planes N(1)–C(7)–C(6)–C(1)–O(1) (the chelate ring) and N(2)–C(16)–C(10)–C(15)–C(8) (the pendent quinoline group). The dihedral angle between planes O(1)–O(1A)–Ni(1)–N(1)–N(1A) and C(16)–N(2)–C(15)–C(10)–C(9)–C(8)–N(1) is 48.87° showing significant non coplanarity of the NiO_2N_2 plane and the six membered chelate ring formed with the QMP anion and the metal. Aside from the planar complex core the ligands exhibit two further planar parts; i.e. the quinoline moiety and the phenyl moiety, which are both tilted slightly away from the central plane in opposite direction. For the two ligands the quinoline planes are (necessarily) coplanar as are the two phenyl moieties. In the crystal packing each quinoline nitrogen atom, which is not involved in direct bonding is pointing directly to one nickel or cobalt atom of a neighboring molecule creating a pseudo octahedral environment around the metal center, which is exposed to two such functional groups from different neighbors (Fig. 6). The distance between these nitrogen atoms and the nickel centers is 2.973 Å (almost 1 Å longer than the direct Ni–N bond) emphasizing that this is a rather week interaction. By comparing the Ni–O [1.901 Å], Ni–N [2.032 Å] bond distances as well as the Co–O [1.905 Å], Co–N [2.037 Å] bond distances with those in related complexes that do not bear any N-heterocyclic rings, i.e. [1.833 and 1.902 Å] in ($C_{26}H_{24}O_6N_2Ni$) [28] and with [1.913 and 2.007 Å] in ($C_{26}H_{20}CoN_2O_2$) it becomes apparent that the metal chelate core MO_2N_2 is less tightly bound due to the quinoline–metal interactions forming the pseudo-octahedral geometry as shown in Fig. 5 [27,28].

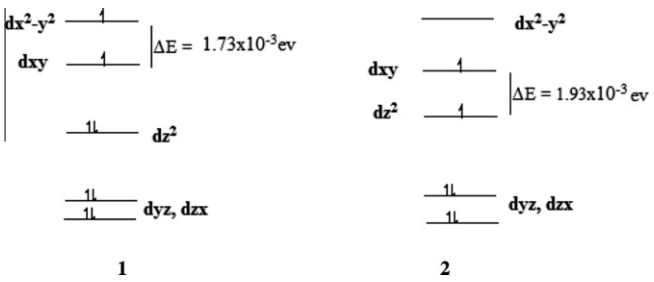

Fig. 2. Crystal field splitting for **1** and **2** on the basis of UV–Vis and $\mu_{effective}$.

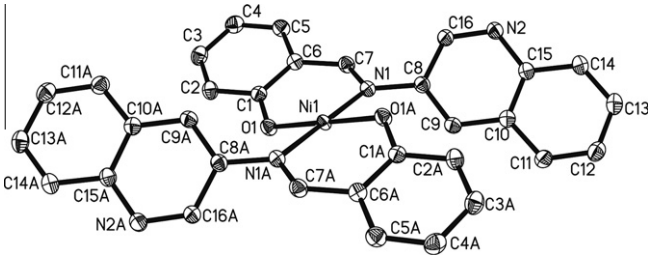

Fig. 3. Molecular structure of **1**. Thermal ellipsoids are shown at 50% probability. H atoms are omitted for clarity reasons. Selected bond lengths [Å] and angles [°]: Ni–O 1.9011(11); Ni–N 2.0323(13); O–Ni–O 180; N–Ni–N 180; O–Ni–N (intra) 90.37(5); O–Ni–N (inter) 89.63(5).

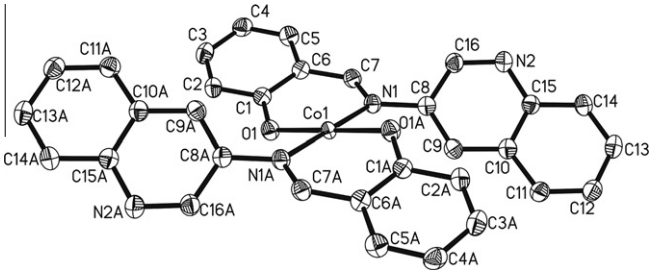

Fig. 4. Molecular structure of **2**. Thermal ellipsoids are shown at 50% probability. H atoms are omitted for clarity reasons. Selected bond lengths [Å] and angles [°]: Ni–O 1.905(11); Ni–N 2.037(13); O–Co–O 180; N–Co–N 180; O–Co–N (intra) 89.55(5); O–Co–N (inter) 90.45(5).

In complex **2** the C(1)–O(1)–Co(1) bond angle is 125.13°, and the C(7)–N(1)–Co(1) bond angle is 120.84° showing little difference to **1**. Similarly the dihedral angle between the planes produced by N(1)–C(7)–C(6)–C(1)–O(1) (the chelate ring) and N(2)–C(16)–C(10)–C(15)–C(8) (the pendent quinoline group) is equal to 28.83° showing the same trend of non coplanarity of the chelate atoms and with the rest of the molecule.

3.2. AChE and BChE inhibition

New cholinesterase inhibitors, in addition to their potential clinical importance if followed by proper pharmacological-investigations, would help in defining the role of BChE in brain development, health and ageing and reveal the value of BChE inhibition as a novel strategy for the treatment of AD [7]. Here, we report the AChE and BChE inhibition capabilities of the four synthesized metal complexes and their mutual relationships (Table 1). All compounds were found inactive against acetylcholinesterase. The cobalt and copper QMP complexes were shown to be selectively inhibiting BChE, whereas the remaining compounds are inactive. It was previously reported that during the development of AD the activity of BChE increases by 40–90%. Examination of the amyloid plaque also show the increased concentration of BChE [35,36]. Therefore the selective BChE inhibitors like copper and cobalt QMP complexes may be good therapeutic agents. It has been shown that the amyloid protein precursor (APP) possesses specific selective Zn^{2+} and Cu^{2+} binding sites which mediate its physicochemical behavior and if occupied, may cause inhibition of AChE and BChE [29]. BChE inhibitors have been used to delay symptoms of AD patients by virtue of their ability to enhance acetylcholine availability. Their involvement in a cholinergic anti-inflammatory pathway connect BChE and AChE with a possible marker of low-grade systemic inflammation observed in Type-2 diabetes, obesity, hypertension, coronary heart disease, and AD [30,31]. Thus, new metal based inhibitors for BChE are among the most sought after targets for therapeutic use in AD treatment [32,33]. Our results, as summarized in Table 1 clearly show that the copper complex is much more active than the cobalt complex, which is in accor-

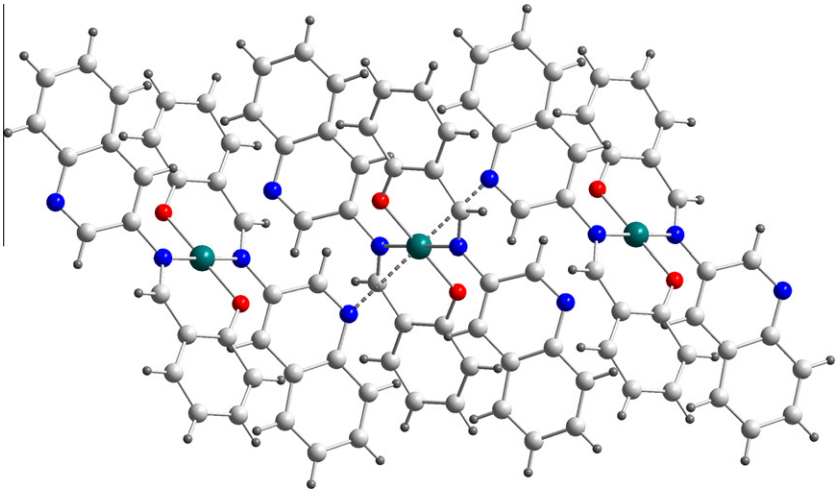

Fig. 5. Intermolecular interactions between quinoline nitrogens and nickel in the crystal structure of **1** leading to the pseudo-octahedral coordination environment of nickel.

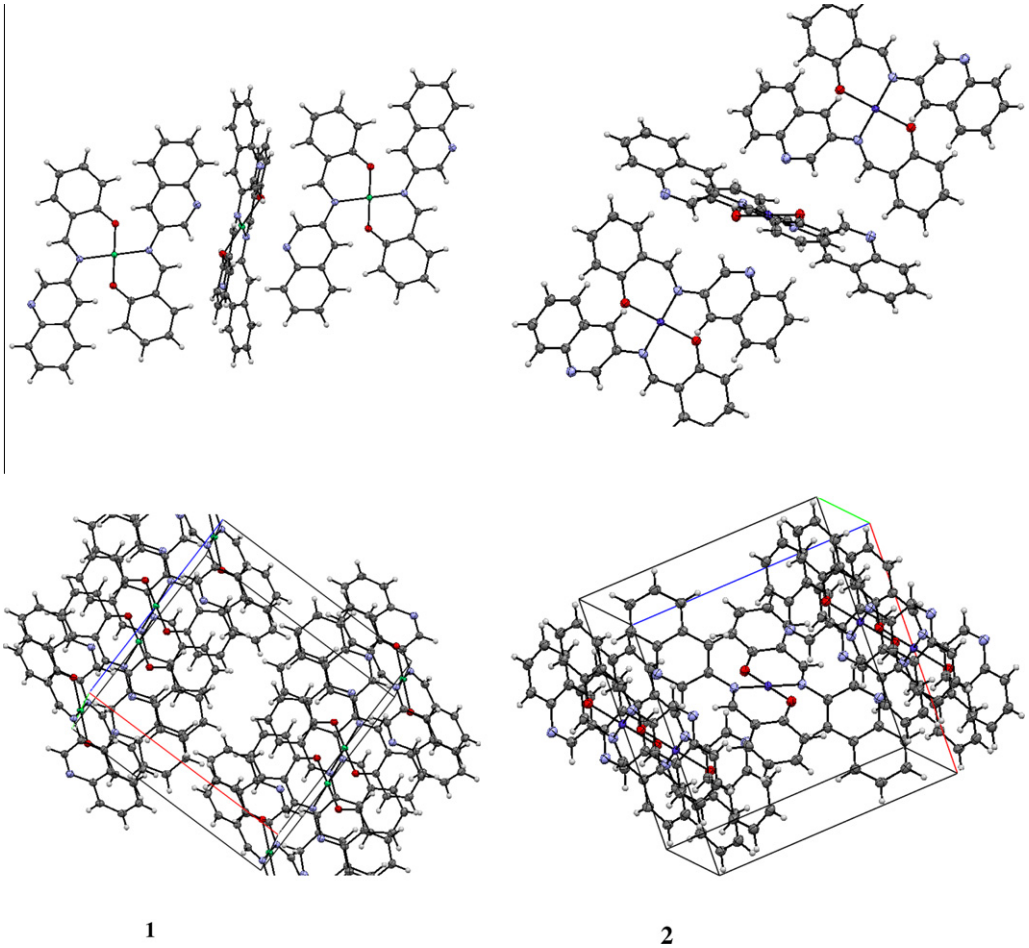

Fig. 6. Crystal packing diagrams for **1** and **2**.

dance with senile plaque naturally containing copper. Due to the abundance of copper in particular in the brain, complexes are expected to be actively involved in decreasing the amyloid plaques in AD patients as well as eliminating oxidative stress from proactive metal ions, provided the metal binds at the targeted binding sites of APP [8]. It has been shown with potentiometric and spectroscopic studies that copper coordinates at the N-terminus of the Aβ-peptides, but in equilibrium with the internal histidyl (His13 and His14) sites. The binding based in both cases on the deprotonation of amide groups present on the surface of plaques, but the latter binding mode strongly favors copper over other metal ions [34].

Table 1
In vitro inhibitory activities (in terms of IC_{50} (μM) ± SEM) of H-QMP and its metal complexes against acetylcholinesterase and butyrylcholinesterase.

Sample	Acetylcholinesterase IC_{50} (μM) ± SEM	Butyrylcholinesterase IC_{50} (μM) ± SEM
H-QMP	–	–
1	–	–
2	–	69 ± 0.0112
3	–	5 ± 0.0004
4	–	–
Standard (galanthamine)	8.5 ± 0.5	0.5 ± 0.01

4. Conclusion

The modified aminoquinoline Schiff base ligand was found to produce metal complexes with two different geometries depending on the metal center. The nickel and cobalt complexes were assigned square planar geometries on the basis of spectrometric studies whereas the copper and zinc complex were assigned distorted tetrahedral geometries. The geometries of nickel and cobalt complexes were further confirmed by diffraction studies. The Schiff base and its complexes were studied for acetylcholinesterase and butyrylcholinesterase inhibition activities for a possible therapeutic activity in Alzheimer's disease. The copper and cobalt complexes with QMP were found to be active in inhibiting the butyrylcholinesterase only. This selectivity may be used for designing drugs, which control dementia more specifically and consequently more successfully. The inhibitory concentration needed for the copper complex is considerably lower than for the cobalt complex, emphasizing its superiority in this respect, which is in accordance with previous metal to Aβ binding studies and the natural abundance of copper in the brain. Here, we have shown that the easily accessible QMP^- ligand in combination with copper might be reasonable alternative drugs, which have been used and are being used for the inhibition of butyrylcholinesterase in order to treat Alzheimer's disease and for related illnesses.

Acknowledgment

The authors Muhammad Ikram and Sadia Rehman gratefully acknowledge the Higher Education Commission (HEC) Pakistan for providing the indigenous and IRSIP scholarships for this work.

Appendix A. Supplementary material

CCDC 853083 and 853082 contain the supplementary crystallographic data for compounds **1** and **2**, respectively. These data can be obtained free of charge from The Cambridge Crystallographic Data Centre via www.ccdc.cam.ac.uk/data_request/cif. Supplementary data associated with this article can be found, in the online version, at http://dx.doi.org/10.1016/j.ica.2012.04.036.

References

[1] H. Sugimoto, H. Ogura, Y. Arai, Y. Iimura, Y. Yamanishi, Jpn. J. Pharmacol. 89 (1) (2002) 7.
[2] J.L. Sussman, M. Harel, F. Frolow, C. Oefner, A. Goldman, L. Toker, I. Silman, Science 253 (5022) (1991) 872.
[3] M.H. Parker, A.B. Reitz, Chemtracts: Org. Chem. 13 (1) (2000) 51.
[4] G.M. Shankar, S. Li, T.H. Mehta, A. Garcia-Munoz, N.E. Shepardson, I. Smith, F.M. Brett, M.A. Farrell, M.J. Rowan, C.A. Lemere, C.M. Regan, D.M. Walsh, B.L. Sabatini, D.J. Selkoe, Nat. Med. 14 (8) (2008) 837.
[5] S. Nochi, N. Asakawa, T. Sato, Biol. Pharm. Bull. 18 (1995) 1145.
[6] W. Tong, E.R. Collantes, Y. Chen, W.J. Welsh, J. Med. Chem. 39 (1996) 380.
[7] Q. Yu, H.W. Holloway, T. Utsuki, A. Brossi, N.H. Greig, J. Med. Chem. 42 (1999) 1855.
[8] N.H. Greig, T. Utsuki, Q. Yu, X. Zhu, H.W. Holloway, T. Perry, B. Lee, D.K. Ingram, D.K. Lahiri, Curr. Med. Res. Opin. 17 (2001) 159.
[9] M. Racchi, M. Mazzucchelli, E. Porrello, C. Lanni, S. Govoni, Pharmacol. Res. 50 (4) (2004) 441.
[10] P. Camps, D. Muñoz-Torrero, Mini-Rev. Med. Chem. 2 (1) (2002) 11.
[11] N. Tezer, J. Mol. Struct. (Thoechem.) 714 (2–3) (2005) 133.
[12] H. Haviv, D.M. Wong, I. Silman, J.L. Sussman, Curr. Top. Med. Chem. 7 (4) (2007) 375.
[13] H. Dvir, D.M. Wong, M. Harel, X. Barril, M. Orozco, F.J. Luque, D. Munoz-Torrero, P. Camps, T.L. Rosenberry, I. Silman, J.L. Sussman, Biochemistry 41 (9) (2002) 2970.
[14] G. Evin, G. Lessene, S. Wilkins, Recent Pat. CNS Drug Discovery 6 (2) (2011) 91.
[15] M. Harel, I. Schalk, L. Ehretsabatier, F. Bouet, M. Goeldner, C. Hirth, P.H. Axelsen, I. Silman, J.L. Sussman, Proc. Natl. Acad. Sci. U S A 90 (1993) 9031.
[16] G. Koellner, G. Kryger, C.B. Millard, I. Silman, J.L. Sussman, T. Steiner, J. Mol. Biol. 296 (2) (2000) 713.
[17] S. Alcaro, L. Scipione, F. Ortuso, S. Posca, V. Rispoli, D. Rotiroti, Bioorg. Med. Chem. Lett. 12 (20) (2002) 2899.
[18] M.M. Hurley, J.B. Wright, G.H. Lushington, W.E. White, Theoret. Chem. Acc. 109 (3) (2003) 160.
[19] Y.K. Zhang, J. Kua, J.A. McCammon, J. Am. Chem. Soc. 124 (35) (2002) 10572.
[20] M.L. Bolognesi, M. Bartolini, A. Cavalli, V. Andrisano, M. Rosini, A. Minarini, C.D. Melchiorre, J. Med. Chem. 47 (24) (2004) 5945.
[21] A.A.N. de Paula, J.B.L. Martins, M.L. dos Santos, L.D. Nascente, L.A.S. Romeiro, T. Areas, K.S.T. Vieira, N.F. Gamboa, N.G. Castro, R. Gargano, Eur. J. Med. Chem. 44 (9) (2009) 3754.
[22] (a) A. Budimir, N. Humbert, M. Elhabiri, I. Osinska, M. Biruš, A.M. Albrecht-Gary, J. Inorg. Biochem. 105 (3) (2011) 490;
(b) A. Rimola, J. Alí-Torres, C. Rodríguez-Rodríguez, J. Poater, E. Matito, M. Sol, M. Sodupe, J. Phys. Chem. A. 115 (2011) 12659.
[23] H.S. Ved, M.L. Koenig, J.R. Dave, B.P. Doctor, Neuro Rep. 8 (1997) 963.
[24] G.L. Ellman, Arch. Biochem. Biophys. 74 (1958) 443.
[25] G.M. Sheldrick, Acta Crystallogr., Sect. A 64 (2008) 112.
[25] (a) H.B. Gray, C.J. Ballhausen, J. Am. Chem. Soc. 85 (3) (1963) 260;
(b) H.B. Gray, Transition Met. Chem. 1 (1965) 239.
[27] H. Ünver, Z. Hayvalı, Spectrochim. Acta Part A Mol. Biomol. Spectrosc. 75 (2010) 782.
[28] L.W. Juanita, F.M. Selwyn, L. Anders, H. Mikael, J. Susan, Inorg. Chim. Acta 361 (7) (2008) 2094.
[29] I.B. Ashley, Neurobiol. Aging 23 (6) (2002) 1031.
[30] J. Patocka, K. Kuca, D. Jun, Acta Medica. (Hradec Kralove) 47 (4) (2004) 215.
[31] G.F. Makhaeva, A.Y. Aksinenko, V.B. Sokolov, O.G. Serebryakova, R.J. Richardson, Bioorg. Med. Chem. Lett. 19 (19) (2009) 5528.
[32] E. Giacobini, Pharmacol. Res. 50 (2004) 433.
[33] N.H. Greig, T. Utsuki, D.K. Ingram, Y. Wang, G. Pepeu, C. Scali, Q.S. Yu, J. Mamczarz, H.W. Holloway, T. Giordano, D. Chen, K. Furukawa, K. Sambamurti, A. Brossi, D.K. Lahiri, Proc. Natl. Acad. Sci. U S A 102 (2005) 17213.
[34] É. Józsa, K. Ősz, C. Kállay, P. de Bona, C.A. Damante, G. Pappalardo, E. Rizzarelli, I. Sóvágó, Dalton Trans. 39 (2010) 7046.
[35] N.H. Greig, K. Sambamurti, Q.-S. Yu, T.A. Perry, H.W. Holloway, F. Haberman, A. Brossi, D.K. Ingram, D.K. Lahiri, Butyrylcholinesterase: its selective inhibition and relevance to alzheimer's disease therapy, in: E. Giacobini (Ed.), Butyrylcholinesterase: Its Function and Inhibitors, first ed., Martin Dunitz, Taylor and Francis Group Plc., United Kindom, 2003, p. 69.
[36] C. Geula, S. Darvesh, Drugs Today 40 (2004) 711.